Experimental and modeling study of thermal rate coefficients and cross sections for electron attachment to C 60

Albert A. Viggiano, Jeffrey F. Friedman, Nicholas S. Shuman, Thomas M. Miller, Linda C. Schaffer, and Jürgen Troe

Citation: The Journal of Chemical Physics **132**, 194307 (2010); doi: 10.1063/1.3427530
View online: http://dx.doi.org/10.1063/1.3427530
View Table of Contents: http://scitation.aip.org/content/aip/journal/jcp/132/19?ver=pdfcov
Published by the AIP Publishing

Experimental and modeling study of thermal rate coefficients and cross sections for electron attachment to C_{60}

Albert A. Viggiano,[1] Jeffrey F. Friedman,[1,a)] Nicholas S. Shuman,[1] Thomas M. Miller,[1,b)] Linda C. Schaffer,[1] and Jürgen Troe[2,c)]
[1]*Air Force Research Laboratory, Space Vehicles Directorate, Hanscom Air Force Base, Bedford, Massachusetts 01731-3010, USA*
[2]*Institut für Physikalische Chemie, Universität Göttingen, Tammannstrasse 6, D-37077 Göttingen, Germany*

(Received 8 January 2010; accepted 15 April 2010; published online 18 May 2010)

Thermal electron attachment to C_{60} has been studied by relative rate measurements in a flowing afterglow Langmuir probe apparatus. The rate coefficients of the attachment k_1 are shown to be close to 10^{-6} cm^3 s^{-1} with a small negative temperature coefficient. These results supersede measurements from the 1990s which led to much smaller values of k_1 with a large positive temperature coefficient suggesting an activation barrier. Theoretical modeling of k_1 in terms of generalized Vogt–Wannier capture theory shows that k_1 now looks more consistent with measurements of absolute attachment cross sections σ_{at} than before. The comparison of capture theory and experimental rate or cross section data leads to empirical correction factors, accounting for "intramolecular vibrational relaxation" or "electron-phonon coupling," which reduce k_1 below the capture results and which, on a partial wave-selected level, decrease with increasing electron energy. © *2010 American Institute of Physics*. [doi:10.1063/1.3427530]

I. INTRODUCTION

The attachment of electrons e^- to polyatomic molecules A may involve a series of phenomena. There is, first, the capture of the incoming wave packet of the electrons in the potential of the target molecules. Second, "intramolecular vibrational redistribution (IVR)" or "electron-phonon coupling" may transform the "virtual state" e^-A of the primary capture into an excited anionic state A^{-*}. Third, the metastable anion A^{-*} may rapidly fragment, be radiatively or collisionally stabilized, or autodetach the electron. Inelastic excitation of vibrations of A as well as interference of incoming and outgoing wave packets forming resonances may also play a role. In order to unravel these various contributions, a combination of various types of experiments and theoretical models is required. We have illustrated this for nondissociative and dissociative electron attachment to SF_6 in Refs. 1 and 2. The dependence of thermal attachment rate coefficients k_{at} on the gas temperature T_{gas}, the electron temperature T_{el} (or electron energy E_{el}), and the buffer gas concentration [M] was analyzed by kinetic modeling. A comparison with Vogt–Wannier-type electron capture theory led to empirical information on IVR factors, to be compared with modeling results from R-matrix theory.[3,4] Additional information is obtained from the analysis of attachment cross sections σ_{at} as a function of E_{el} and T_{gas}. However, the sensitivity of the two approaches toward a determination of the IVR factors in practice is different such that it is advantageous to have information from both types of experiments. Finally, thermal attachment[1,2] and detachment[5] rate coefficients are coupled by detailed balancing which, for the case of SF_6, allowed us to redetermine the electron affinity of SF_6. Likewise, attachment cross sections and dissociative lifetimes of energy-selected anions are coupled by detailed balancing and need to be internally consistent.[6–9]

Having demonstrated a combined experimental/theoretical analysis of electron attachment/detachment in the SF_6/SF_6^- system, it appears attractive to treat electron attachment to the much larger molecule C_{60} in a similar fashion. A series of interesting differences are expected. In contrast to SF_6, attachment to C_{60} has been shown to be nondissociative over a very wide electron energy range.[10–12] Note that the C_{60} experiments did not extend to very low energies as with SF_6. Whereas electron attachment to SF_6 is dominated by s-wave capture ($l=0$), the contribution from higher waves (s-, p-, d-, and f-waves, i.e., $l=0$, 1, 2, and 3) was also considered in the theoretical analysis of electron attachment to C_{60}, see Refs. 3 and 4. On the experimental side, an s-wave contribution was assumed at one point not to contribute appreciably. However, more recent work (see, e.g., Refs. 13–22) clearly demonstrated s-wave as well as p-wave contributions to the attachment with additional contributions from higher waves possible. While cross section measurements generally are relative, some absolute determinations have also been made.[13,18,19] These results then were used to attempt a calibration of the relative cross section measurements.[3,4,22] An alternative way to calibrate the cross section data would rely on thermal attachment rates. This approach provided most accurate calibrations for electron attachment to SF_6, see, e.g., Ref. 1. However, thermal attachment studies with varying electron and gas temperatures[23,24] for C_{60} showed a controversial picture.[3,4,11,21] The thermal

a)Permanent address: Department of Physics, University of Puerto Rico, Mayaguez, Puerto Rico 00681-9016.
b)Also at Institute for Scientific Research, Boston College.
c)Electronic mail: shoff@gwdg.de.

attachment rate coefficients from the flowing afterglow-Langmuir probe (FALP) experiments of Refs. 23 and 24 appeared to be consistent with the absolute cross sections from Refs. 18 and 19 only at electron temperatures above about 4000 K. Much lower rate coefficients were observed for lower electron temperatures (see the discussion in Ref. 21). The attachment rates and cross sections, as for SF_6, should also be consistent with measurements of lifetimes of energy-selected C_{60}^- anions, see the storage ring measurements of Ref. 25 and earlier work analyzed in Ref. 9.

The aim of the present study is to shed light on the inconsistency between the thermal attachment rate coefficients from the FALP experiments of Refs. 23 and 24 and cross section data such as described in Refs. 15–22. We again perform FALP experiments, but, in contrast to the absolute rate measurements from Refs. 23 and 24, a relative rate technique was used. We then compare the derived thermal attachment rate coefficients with theoretical capture rate coefficients, accounting for contributions from partial-wave selected capture. This analysis takes advantage of recent analytical approximations for partial-wave selected capture rate coefficients and cross sections from Refs. 26 and 27. In addition, the influence of the large geometrical size of the target C_{60} is inspected on a partial-wave selected level, see Ref. 28. Such effects have been considered before for all-wave capture[21] while partial-wave effects are treated separately for the first time in the present work. Comparing experimental attachment rate coefficients and cross sections with the corresponding data from the mentioned electron capture theory, like for SF_6 in Ref. 1, we try to obtain empirical information on IVR factors for the C_{60} system. Our work focuses attention on the low-energy range relevant for thermal capture rate coefficients, where only few partial waves contribute. A discussion of higher energy effects is less detailed.

II. EXPERIMENTAL TECHNIQUE

The operation of our FALP setup has been discussed in detail previously[29–31] and here we mainly discuss the details important to the present experiment. A plasma is created by a microwave discharge in He which produces He^+, He_2^+, He^* (metastable), and e^- as well as minor concentrations of impurity ions. Ar (~2%) is added downstream of the discharge to convert He_2^+ and He^* into Ar^+ so that the plasma consists of mainly Ar^+ and e^-. He^+ is present at about 5% of the Ar^+ concentration because the buffer gas concentration (3.2×10^{16} cm^{-3}) is not high enough for complete conversion of He^+ to He_2^+. The electron concentration is measured by a movable Langmuir probe. Product ions are monitored by a downstream quadrupole mass spectrometer followed by an analog particle multiplier. An attaching gas is introduced downstream, and traditionally attachment rates are monitored by varying the probe position, which is proportional to the reaction time. However, the traditional method requires that the attaching gas initial concentration is both known and large enough to cause appreciable decay in the electron density along the flow tube. Our method of introducing C_{60} fails on both counts, preventing use of the method employed in Ref. 24, where kinetics of thermal electron attachment to C_{60} was studied under second order conditions and absolute values of the rate coefficient were determined. Instead, we performed relative rate measurements of the reactions of C_{60} and SF_6 with both electrons and Ar^+ and use a calibration reaction to correct for potential mass discrimination.

In order to get a controlled flow of C_{60}, a stainless steel bubbler containing C_{60} was kept at a constant temperature. A controlled He flow through the bubbler carried gaseous C_{60} into the flow tube. Shutting off the He flow lowered the C_{60} concentration below our detection limit. The bubbler reservoir and the tube leading into the flow system were heated separately to about 650 K.

With He flowing through the bubbler, the only appreciable negative ion signal arises from C_{60}^- which is generated by the attachment reaction,

$$e^- + C_{60} \rightarrow C_{60}^- \quad (k_1) \tag{2.1}$$

in which stabilization occurs via a third body or radiation. The C_{60} concentration was found to be approximately proportional to the square root of the He flow rate such as observed also in our previous work for other systems, see Ref. 32. Maintaining a constant flow for approximately 10 min during the course of a data run was essential. We verified this condition by frequently monitoring the C_{60}^- signal which was found to be constant within 10%–20%, well within our error limits. The electron concentration remained essentially unchanged upon C_{60} addition.

Our relative rate method relies on measuring five ion signals for four reactions, where three of the rate constants are known or can be calculated. Besides reaction (2.1), the other reactions of importance are

$$e^- + SF_6 \rightarrow SF_6^- \quad \text{and} \quad SF_5^- + F \quad (k_2), \tag{2.2}$$

$$Ar^+ + C_{60} \rightarrow C_{60}^+ + Ar \quad (k_3), \tag{2.3}$$

and

$$Ar^+ + SF_6 \rightarrow SF_5^+ + F + Ar \quad (k_4). \tag{2.4}$$

Reaction (2.2) has been thoroughly studied using the traditional FALP method (electron depletion versus reaction time).[1,2] Reaction (2.4) has also been investigated over a range of kinetic energies with k_4 being found close to the Langevin collisional limit.[33] We were prevented from measuring reaction (2.4) in the FALP apparatus at high temperature because our flow tube melted and cracked immediately after the present data for the mechanism of reactions (2.1)–(2.4) were taken, in attempting to reach higher temperatures. However, Ar^+ reactions such as reaction (2.4) inevitably stay near to the collisional value.[34,35] Reaction (2.3) has been observed in Ref. 36, but its rate coefficient is unknown. However, exothermic charge transfer reactions with large molecules usually occur at the collisional rate. For instance, our laboratory has measured the rate coefficients of the reaction of Ar^+ with benzene[37] and naphthalene[38] which are close to the collisional value up to very high temperature. Therefore, it appears most reasonable to assume that the rate coefficient for reaction (2.3) is essentially the Langevin collisional value. There remains a small but unknown amount of He^+ in the system which is not converted to Ar^+. The chem-

istry of this species is mostly similar to that of Ar^+ except that some SF_3^+ and C_{60}^{2+} are formed. Those signals are small enough to be neglected within our uncertainty.

The experiments were run as follows, with the order of the measurements being unimportant. First, the ambipolar diffusion rate was determined by measuring the electron density decay along the flow tube axis in absence of reactant gas. Then, the ion signals of C_{60}^-, $SF_6^-+SF_5^-$, C_{60}^+, and SF_5^+ were determined. The C_{60}^- and C_{60}^+ intensities were measured with a constant He flow through the bubbler. The bubbler flow was then turned off and a known flow of SF_6 was added to a separate inlet with the distance (and therefore, reaction time) between the inlets known. The SF_6 concentration was chosen so that the $SF_6^-+SF_5^-$ signal was on the same order as the C_{60}^- signal. The concentration of SF_6 in the flow tube was adjusted as low as 2×10^7 cm^{-3} or 0.6 parts per billion. Positive ion spectra were then measured with the same C_{60} and SF_6 concentrations, so that C_{60}^+ and SF_5^+ signals were obtained. By this procedure, relative concentrations of $C_{60}^+:SF_5^+$ and $C_{60}^-:(SF_6^-+SF_5^-)$ were measured.

The rate coefficients for electron attachment to C_{60} were determined through the analysis of the kinetics of the system described by the reactions (2.1)–(2.4), employing the measured initial electron concentrations, which equals the initial Ar^+ concentration. Product concentrations were calculated by integration of the kinetic equations over the investigated maximum reaction time (about 5 ms) with the time zero corresponding to the ion flow at the upstream inlet port (through which the SF_6 is introduced; C_{60} was introduced at the downstream port about 1.5 ms later). Besides the rates of reactions (2.1)–(2.4), our integration accounted for the experimentally measured ambipolar diffusion of e^- and Ar^+. SF_5^+ and C_{60}^+ were treated as diffusing at the limiting values of either the Ar^+ rate or not at all (being considerably more massive than Ar^+) in order to judge the uncertainty associated with diffusion. Negative ions are assumed not to diffuse until the electron population is depleted, a condition never reached here.

With known initial SF_6 and electron concentrations, the treatment of the kinetics yields the SF_5^+ and $SF_6^-+SF_5^-$ concentrations at the maximum reaction time, i.e., at the mass spectrometer sampling orifice. The measured $(SF_6^-+SF_5^-)/C_{60}^-$ and SF_5^+/C_{60}^+ ratios (corrected for instrumental mass discrimination) then led to the C_{60}^- and C_{60}^+ concentrations at the sampling orifice. The remaining unknowns, the attachment rate coefficient k_1, and the initial C_{60} neutral concentration were determined by iteratively varying these two quantities until agreement with the relative mass spectral intensities was obtained. Alternatively, under the assumption that both the electron and Ar^+ concentrations are always in large excess, the $(SF_6^-+SF_5^-)/SF_6^+$ ratio is determined by the ratio of k_2 and k_4, which fixes the C_{60}^-/C_{60}^+ ratio (via the measured ion ratios) independent of both the initial SF_6 and C_{60} neutral concentrations and yields the C_{60} electron attachment rate coefficient k_1 relative to the collisional rate coefficient for charge transfer from Ar^+ to C_{60}. As long as the SF_6 and C_{60} concentrations are much lower than the electron concentration, the derived attachment parameters do not depend on the initial concentrations of either SF_6 or C_{60}.

The main source of error in this technique is potential mass discrimination. For our instrument, we have found large corrections needed at low masses (i.e., for F^- and Cl^-), but little correction above 80 amu, up to at least 300 amu (ReF_6^-). We observe a difference in the detection of atomic ions versus molecular ions, presumably due to the secondary emission coefficient from collisions with the 4 kV-conversion dynode of our electron multiplier, but little difference for heavy molecular ions. However, it is not discrimination between ions of one sign but the *difference* in mass discrimination between positive and negative ions that matters. Discrimination between ions of one sign leads only to a faulty C_{60} concentration determination. As long as the discrimination between SF_6^- and C_{60}^- is the same as that between SF_5^+ and C_{60}^+, the faulty concentration cancels in determining the electron attachment rate constant (provided that electrons are not appreciably depleted by the very small concentrations of SF_6 or C_{60}).

In order to calibrate this relative mass discrimination, we substituted C_7F_{14} (the heaviest species we can reliably get into the flow tube and for which all needed rate constants are known)[39,40] for C_{60} and ran both relative rate and traditional electron depletion experiments to measure the C_7F_{14} attachment rate constant. These results showed that the higher mass is discriminated against by a larger factor (1.9) when monitoring negative ions compared to monitoring positive ions. The technique is not perfect because the reaction does not cover the range up to the C_{60} mass of 720 amu, and the correction represents an upper bound because charge transfer with Ar^+ partially fragments the C_7F_{14}. The factor of 1.9 is used as a final correction to the C_{60} attachment rate coefficient determined using the present relative rate method.

Given the difficulty of the experiments, we estimate a maximum uncertainty of a factor of 3 in the absolute C_{60} attachment rate coefficients. However, most of the potential error is temperature independent, and the relative error between the 400 and 625 K results is estimated to be considerably lower, being about ±40%. We feel that our factor of 3 uncertainty is adequate because (1) only discrimination differences between positive versus negative ion discrimination matters and (2) our calibration technique with C_7F_{14} yielded a correction that is considerably smaller than this estimated uncertainty.

III. EXPERIMENTAL RESULTS

Figure 1 shows an example of calculated concentration profiles in an experiment at 400 K. Here, C_{60} was added 1.5 ms later than SF_6, thus showing a delayed onset in the figure. The initial SF_6 concentration was 2.0×10^7 cm^{-3} and the initial C_{60} concentration was the maximum we could introduce to the flow tube at 400 K (on the order of 10^6–10^7 cm^{-3}). At 625 K, a comparable amount of SF_6 was added and a higher C_{60} concentration of $\sim10^7$ cm^{-3} was reached. The concentrations of Ar^+ and e^- were practically unaffected by such low reactant concentrations, and these two species were lost mainly by diffusion. Note that Fig. 1

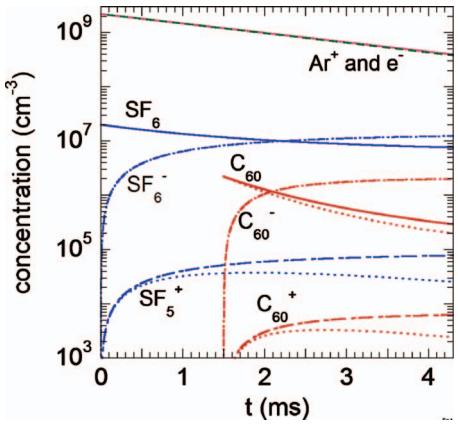

FIG. 1. Calculated concentration vs time profiles of various species in the flow tube for a typical experiment at 400 K (the shift between the C_{60}- and SF_6-related profiles is due to the addition of C_{60} at 1.55 ms later than SF_6, see text). The curve labeled SF_6^- represents the sum $SF_5^-+SF_6^-$. The C_{60}^+ and SF_5^+ concentrations are shown with two limiting assumptions, no diffusion (broken curve) and with diffusion (dotted curve); the latter requires a higher $k_{at}(C_{60})$ to fit the relative positive ion intensities measured at the end of the flow tube (4.3 ms). The Ar^+ (solid line) and e^- (dashed line) concentrations are almost indistinguishable because they decay mostly by ambipolar diffusion and only very slightly due to reaction.

covers more than six orders of magnitude in concentration. The SF_6 concentration decays by almost a factor of 7, predominantly because of the attachment reaction (2.2). At the end of the flow tube, the SF_6^- concentration is almost equal to the starting SF_6 concentration, while the SF_5^- concentration is unimportant at 400 K. The SF_5^+ concentration increases due to reaction (2.4) and may decrease at longer times due to diffusion. The SF_6 concentrations are calculated without adjustable parameters and the end values are combined with the measured ion ratios to derive C_{60}^- and C_{60}^+ concentrations at the sampling orifice. For C_{60} addition, the same characteristics are observed after accounting for the delayed introduction of C_{60}. Both C_{60}^- and C_{60}^+ ion concentrations are about an order of magnitude smaller than the ion concentrations produced from SF_6. Fits to the mass spectral data are sensitive to variations of only 10% in the derived quantities, leaving uncertainty in the measured ion intensities (including relative mass discrimination) the dominant factor in the reported error limit.

Table I lists the experimental ion ratios and the attachment rate coefficients k_1. As discussed above, the k_1 were determined under the limiting conditions that the heavy positive ions diffuse at the same rate as Ar^+ or do not diffuse at all. The C_{60} concentrations derived are about 2.2 and 13 $\times 10^6$ cm^{-3} at 400 and 625 K, respectively, but these figures are subject to large uncertainty, as explained above. The rate coefficients are large, being $\sim 10^{-6}$ cm^3 s^{-1}. The 400 K values are about 1.6 times larger than those at 625 K. This corresponds to a temperature dependence of $k_1 \propto T^{-1}$ independent of which assumption is made regarding heavy-ion diffusion. Using the 40% relative uncertainty shows that the temperature exponent is uncertain by a factor of 3.

The previous FALP study of thermal electron attachment to C_{60} from Refs. 23 and 24 relied on absolute rate measurements under second order conditions. The attachment rate coefficients were measured as a function of the electron temperature T_{el}. The C_{60} concentration was determined only once at $T_{el} \approx 4500$ K in a pure Ar buffer held at $T_{gas} = 300$ K. Afterwards, He was added to the buffer to reduce T_{el}. At high T_{el}, a value of $k_1 \approx 3 \times 10^{-7}$ cm^3 s^{-1} was found, which within the uncertainties is in agreement with the present values obtained for $T_{el}=T_{gas}$. However, the measurements of Refs. 23 and 24 led to much lower values of k_1 at smaller T_{el}, e.g., $k_1=3\times10^{-9}$ cm^3 s^{-1} at $T_{el} \approx 500$ K, which is in marked contrast to the present results. The experiments of Refs. 23 and 24 were made in the days before C_{60} was inexpensive and commercially obtainable and were carried out with only 10 mg of C_{60} available. The sample was heated in a boat located in the flow tube and was consumed at an estimated rate of 1 mg/min, but it was assumed that the amount of C_{60} remained constant after the initial measurement. Considering the available quantity of original material and the rate of use, that would seem a questionable assumption. Based on the present measurements which led to large values of k_1 at both 400 and 625 K, we speculate that the T_{el} dependence was the result of a rapid change in the C_{60} concentration in time, either due to sample depletion or that the He flow introduced to vary T_{el} slightly cooled the boat. In either case, the apparent rate coefficient would decrease with time. Were C_{60} readily available, measurements of the concentration could have been made for every condition. Our method of introducing C_{60} into the flow tube did not yield high enough concentrations to permit us to repeat the earlier FALP measurements; therefore, we used the relative rate method with $T_{el}=T_{gas}$. For the reason given above, we believe that the present results correspond to much better defined conditions than those applied in Refs. 23 and 24. This is confirmed by the comparison of the derived rate coefficients with data calculated from cross section measurements such as shown in Sec. IV.

IV. MODELING OF ATTACHMENT CROSS SECTIONS AND THERMAL RATE COEFFICIENTS

We start the modeling part of the present article by considering capture of electrons in the polarization potential of

TABLE I. Cation and anion concentration ratios and thermal rate coefficients k_1 for electron attachment to C_{60} at 400 and 625 K ("diff" and "no diff" refer to whether heavy positive ions were assumed to diffuse or not to diffuse, see text). Given the large uncertainty (factor of 3) estimated for k_1 due to instrumental mass discrimination, the positive ion diffusion issue (see text) is unimportant and average values 1.2×10^{-6} (400 K) and 8×10^{-7} cm^3 s^{-1} (625 K) are recommended. The relative error between these two values is estimated at ±40%.

T (K)	$[C_{60}^+]/[SF_5^+]$	$[C_{60}^-]/([SF_6^-]+[SF_5^-])$	k_1(diff) (cm^3 s^{-1})	k_1(no diff) (cm^3 s^{-1})
400	0.13	0.14	1.4×10^{-6}	1.1×10^{-6}
625	1.05	0.76	9.0×10^{-7}	6.6×10^{-7}

C_{60} whose polarizability is taken as $\alpha=76.5(\pm 8)\times 10^{-24}$ cm^3, see Refs. 41–43. By comparison with experimental results for attachment cross sections and rate coefficients, then empirical IVR factors are derived. We do our modeling first for C_{60} treated as a zero-size target species. We then compare the results with a modeling for finite-size C_{60} having a geometrical radius of $r_0=0.354(\pm 0.001)$ nm such as derived in Refs. 43 and 44.

We identify the nondissociative attachment cross section σ_{at} with the capture cross section σ_{cap} and express the latter in the form[1]

$$\sigma_{cap}=(\pi/k^2)\sum_{l=0}^{\infty}(2l+1)P_l^{IVR}P_l^{VW}(k), \tag{4.1}$$

where k denotes the wave vector $k=p/\hbar=(2\mu E_{el}/\hbar^2)^{1/2}$, E_{el} is the kinetic energy of the electrons, $P_l^{VW}(k)$ are partial wave, l, selected capture probabilities within the Vogt–Wannier approach,[3,4,26–28] and the P_l^{IVR} are IVR probabilities which besides l may depend on T_{gas} and E_{el} (or T_{el}), see our analysis of electron attachment to SF_6 in Ref. 1. For a zero-size species, the $P_l^{VW}(k)$ within the Vogt–Wannier approach have been calculated numerically (up to $l=3$) and presented graphically in Refs. 3 and 4. In addition, approximate analytical expressions (up to $l=12$) were designed in Refs. 26–28. For convenience, we have used the latter relationships. Partial-wave selected finite-size modifications of the $P_l^{VW}(k)$, as well as approximate expressions for the $P_l^{VW}(k)$ at $l>12$, have also been developed recently[28] and are applied to C_{60} in the present work. If C_{60} could be treated classically on an all-wave level, the capture cross section could be expressed as[21]

$$\sigma_{cap}^{cl}=\pi r_0^{\,2}+(2\pi^2 e^2\alpha/E_{el})^{1/2}, \tag{4.2}$$

with $\pi r_0^{\,2}=0.394$ nm^2 (instead of the $\pi r_0^{\,2}=0.79$ nm^2 used in Ref. 21). Equation (4.2) applies to high energies where many partial waves contribute. At low energies, Eq. (4.2) ceases to be valid. Quantum effects increase $P_{l=0}^{VW}$ by up to a factor of 2 beyond the corresponding classical Langevin value at low energies, see Refs. 26–28. On the other hand, finite-size effects diminish for decreasing l, see Ref. 28.

Making use of the theoretical work of Ref. 28, we modeled capture cross sections [i.e., putting $P_l^{IVR}=1$ in Eq. (4.1)] for zero-size and real-size C_{60}. Figure 2 shows the results. Partial-wave selected capture cross sections $\sigma_{cap,l}$ defined by

$$\sigma_{cap,l}=(\pi/k^2)(2l+1)P_l^{VW}(k) \tag{4.3}$$

are presented together with total capture cross sections σ_{cap} from Eq. (4.1). The only minor importance of the finite size of C_{60} for small l is illustrated both for $\sigma_{cap,l}$ and for σ_{cap}. Finally, it is shown that the classical cross section of Eq. (4.2) with increasing energy, both for zero-size and finite-size C_{60}, is quickly approached by σ_{cap}. Only below $E_{el}=0.01$ eV will the quantum effects in $\sigma_{cap,l=0}$ lead to $\sigma_{cap}>\sigma_{cap}^{cl}$. However, some quantum oscillations around the classical cross sections can also be noticed in the figure.

A comparison of the modeled σ_{cap} with measured attachment cross sections σ_{at} should give some information on the IVR factors P_l^{IVR}. There are only very few absolute determinations of σ_{at} at sufficiently low energies. The measurements of Refs. 18 and 19 are among them and we make use of these results. Figure 3 provides the comparison of the modeled σ_{cap} and the measured σ_{at}. An inspection of Fig. 2 suggests that, for the given energy range up to 0.35 eV, not only s- and p-waves[3,4,15,22] but also higher partial waves have to be taken into consideration which has been done in Fig. 3 (including l up to 100). The figure shows the corresponding capture cross sections σ_{cap}. The experimental points for σ_{at} from Refs. 18

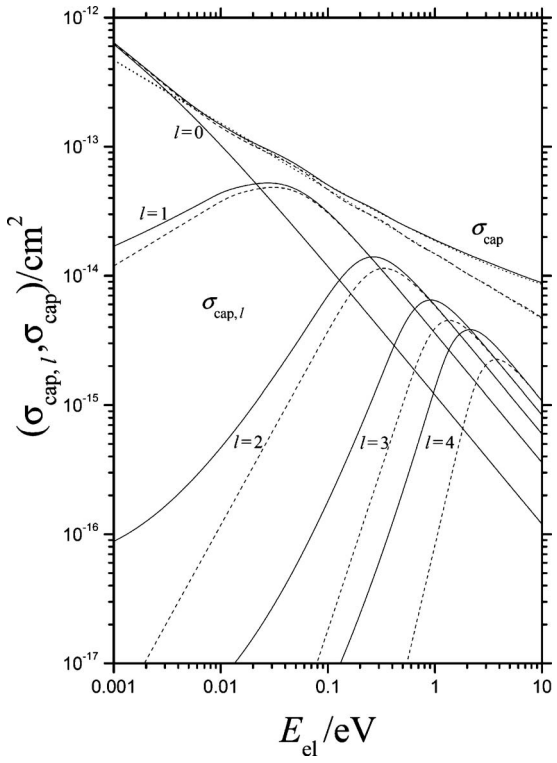

FIG. 2. Modeled cross sections σ_{cap} for electron capture by C_{60} as a function of the electron energy E_{el}. Partial waves are separated ($\sigma_{cap,l}$ with $l=0,\ldots,4$) or summed up ($\sigma_{cap,l}$ with $l\rightarrow 100$) [full lines=modeling with finite-size C_{60}, dashed lines=modeling with zero-size C_{60}, dotted line =classical finite-size Langevin cross section σ_L of Eq. (4.2)].

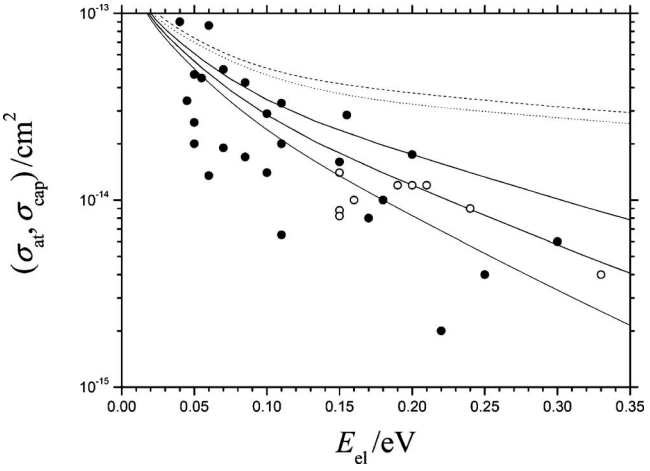

FIG. 3. Comparison of modeled capture and attachment cross sections without IVR (σ_{cap} with $c_1=0$, dashed line=finite-size C_{60}, dotted line =zero-size C_{60}) and with IVR [σ_{at} with full lines for $c_1=0.10$, 0.15, and 0.20 in Eq. (4.5) from top to bottom] with measured attachment cross sections from Refs. 18 (open points) and 19 (solid points), see text.

and 19 are below σ_{cap}, as they should be. In addition, a comparison of Figs. 2 and 3 clearly indicates that an s-wave contribution could only be identified if measurements could be resolved down to energies below 0.02 eV, see below.

The difference between σ_{cap} and σ_{at} in our analysis is expressed in terms of the "IVR factors." At this stage, they are empirical factors to be interpreted by more detailed theory such as R-matrix theory when this becomes possible. They are useful parameters when kinetic quantities such as cross sections, rate coefficients, and detachment lifetimes are related. However, at present, only vague information on these factors is available. For the s-wave dominated electron attachment to SF_6, a functional form of the type

$$P_{l=0}^{IVR} \approx \exp(-c_1\kappa^2) \tag{4.4}$$

[with $\kappa=\mu e(2\alpha E_{el})^{1/2}/\hbar^2$] was suggested, with parameters c_1 which may depend on the buffer gas temperature T_{gas}. For electron attachment to SF_5Cl, a similar relation was found to apply,[45] however, with an additional, potentially temperature dependent, factor A in front of the exponential. In both cases, at large energies $P_{l=0}^{IVR}$ was found to level off at some nonzero value which is not included in Eq. (4.4). For C_{60}, we are clearly not in the position to provide partial-wave selected information on the IVR factors P_l^{IVR}. However, the comparison of modeled capture cross sections and the measured attachment cross sections from Refs. 18 and 19 in Fig. 3 suggests that P^{IVR} decreases with increasing electron energy similar as given by Eq. (4.4). An experimental justification for this procedure is given in the following. For simplicity, we assume $P_{l=0}^{IVR}$ to be of the form of Eq. (4.4) independent of T_{gas}. For $l>0$, again for simplicity we extend Eq. (4.4) to a form

$$\begin{aligned} P_l^{IVR} &= 1 && \text{for } \kappa < \kappa_0(l) \\ &= \exp[-c_1(\kappa^2 - \kappa_0^2(l))] && \text{for } \kappa \geq \kappa_0(l), \end{aligned} \tag{4.5}$$

where κ_0 corresponds to the centrifugal barriers of the orbiting potential between C_{60} and the electrons. Following Ref. 28, for finite-size C_{60} this is calculated to be

$$\kappa_0^2(l) = \{l(l+1)/[\sqrt{1+l(l+1)(r_0/1.202\ \text{nm})^2}+1]\}^2. \tag{4.6}$$

The parameter c_1 then is chosen in such a way that the experimental attachment cross sections from Refs. 18 and 19 and the thermal attachment rate coefficients $k_{at}=k_1$ from the present work are reproduced consistently. Within the rather large experimental uncertainties, this is achieved by choosing

$$c_1 \approx 0.2 \tag{4.7}$$

independent of the buffer gas temperature. Figure 3 includes modeled curves with $c_1=0.1$, 0.15, and 0.2, in order to illustrate the dependence of the results on the IVR factor.

Different conclusions on the IVR factors were drawn in Refs. 4 and 22 where measured relative cross sections from Refs. 16 and 22 as well as absolute cross sections from Refs. 13 and 18 were represented in the form

$$\sigma_{at} = c(\varepsilon\sigma_{cap,l=0} + \sigma_{cap,l=1}). \tag{4.8}$$

With $c\approx0.1$ and $\varepsilon\approx0.1$ from Ref. 4, this leads to $P_{l=0}^{IVR} \approx 0.01$ and $P_{l=1}^{IVR}\approx0.1$, while $c\approx0.06$ and $\varepsilon\approx0.45$ were derived in Ref. 22 which corresponds to $P_{l=0}^{IVR}\approx0.027$ and $P_{l=1}^{IVR}\approx0.06$. The parameter ε in Eq. (4.8) characterizes the ratio of the contributions of s- and p-waves while the parameter c assures the absolute calibration of the cross sections. The differences in ε between Ref. 4 and 22 are directly related to the differences of the heights of the experimental zero energy peaks of the cross sections, with Ref. 4 relying on Ref. 16, and Ref. 22 on its own results which were obtained later than those of Refs. 16 and 4. Figure 2 indicates that the s-wave peak is very narrow and has a calculated width of only about 5 meV; and the minimum of the sum of the s- and p-wave cross section is located near 20 meV. The experimental energy resolution was much larger, e.g., 130 meV in Ref. 22. It is thus difficult to derive the true height of the zero energy peak from the low resolution experiments. In Ref. 4, the Vogt–Wannier capture cross sections were convoluted with the experimental energy distributions and the parameter ε then was optimized by comparison with the low resolution experimental data over the range 0–0.5 eV. One has to ask whether the narrow s-wave peak at 0 eV can be accurately portrayed by this procedure when the experimental resolution is more than ten times the peak width. In this context one should also note that the experimental relative ion yields I(0 eV)/I(1 eV) in different experiments with different resolutions vary between values near unity and more than 10.[17,19,20] In the present work, we relied on the experiments from Refs. 18 and 19 which had the best energy resolutions and the highest ratios I(0 eV)/I(1 eV) such as illustrated in Fig. 3. If an energy independent IVR factor such as in Refs. 4 and 22 would be chosen, Fig. 3 would lead to similar ε values as obtained in these references. However, this would lead to much smaller thermal rate coefficients than measured in our work, see below. In fact, the thermal rate coefficients measured at 400–600 K are much more sensitive to the details of the low energy behavior than the measured cross sections. The consequence of our combined analysis of measured attachment cross sections and rate coefficients therefore leads one to conclude that the IVR factor has an energy dependence. We chose the form to be analogous to the SF_6 system, given by Eqs. (4.4)–(4.7). The second parameter c in Eq. (4.8) provides the absolute calibration of relative cross section data. In Ref. 22 it was fixed by the absolute cross section value at 1 eV from Refs. 13 and 18 However, when absolute cross sections near 0 eV are of importance, such as this is the case for the present thermal rate coefficients, data near 1 eV do not appear sufficient to conclude on the product of the parameters c and ε and its energy dependence. Nevertheless, the present approach also considers cross sections near 1 eV and shows a semiquantitative consistency with the absolute data from Refs. 13 and 18, see below. In addition, it relies more strongly on the absolute cross sections at low energies from Ref. 19, see Fig. 3.

Thermal averaging of the capture cross sections, following the procedure outlined in Ref. 46, leads to thermal capture and attachment rate coefficients. Figure 4 shows the re-

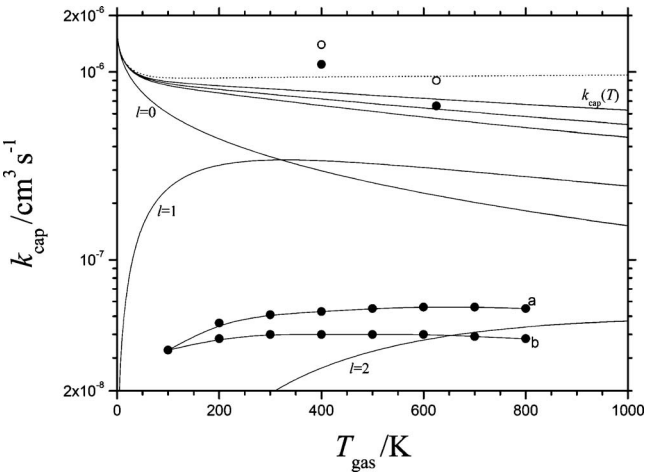

FIG. 4. Thermal rate coefficients for capture and attachment of electrons k_{cap} by C_{60} (full lines) for $l=0$, 1, and 2: capture by separate s-, p-, and d-waves employing IVR factors from Eqs. (4.4) and (4.5) with $c_1=0.2$; full lines with points: deconvolution of experimental attachment cross sections performed in Refs. 4 (a) and 22 (b); upper full lines for $k_{cap}(T)$: modeling of attachment rate coefficients employing IVR factors with $c_1=0.1$, 0.15, and 0.2 from top to bottom; dotted line: calculation of $k_{cap}(T)$ with $c_1=0$; solid points at top: experimental results from this work neglecting diffusion; open points at top: experimental results including diffusion of heavy positive ions (see text).

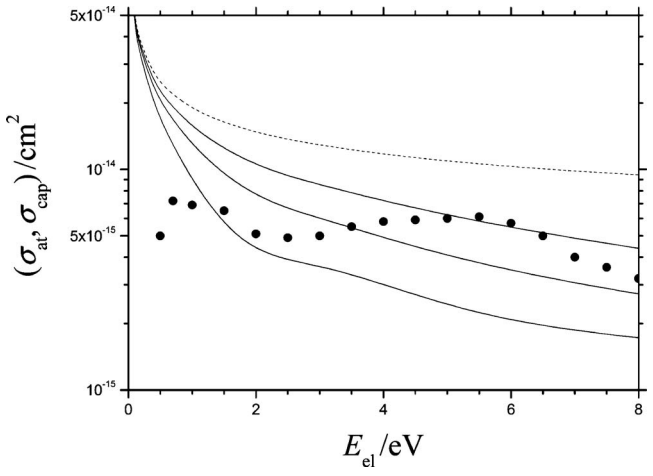

FIG. 5. Modeled capture cross sections σ_{cap} (lines) in comparison to measured attachment cross sections σ_{at} (circles: summary of experiments given in Ref. 21). The figure extends Fig. 3 to higher energies [dashed line: IVR factor $P^{IVR}=1$, full lines from top to bottom: IVR factors from Eqs. (4.5) and (4.6) with the parameters $c_1=0.005$, 0.01, and 0.02].

sults. Up to 1000 K, mostly s- and p-waves ($l=0$ and 1) contribute, but the figure indicates also a small d-wave ($l=2$) component. The individual s-wave and p-wave contributions have different temperature coefficients, such as illustrated in the figure. Our measured values of k_1, independent of including or excluding diffusion (see above), are close to the capture rate coefficients without accounting for IVR. However, because the thermal experiments sample only very low electron energies, the IVR effects are still small and the experimental uncertainty prevents us from determining the IVR parameter c_1 precisely. Nevertheless, one may say that c_1 is smaller than or of the order of 0.2. The cross section measurements of Fig. 3 sample slightly higher energies where IVR factors are more pronounced and can be identified somewhat more easily. These data led to values of c_1 of the order of 0.2 which appears still compatible with the present experiments. The two sets of data thus appear consistent with each other. This consistency would not be obtained if the cross sections would be as small as suggested by Refs. 4 and 22. Then, the thermal rate coefficients should have been about a factor of 20 smaller than measured in the present work. This is illustrated in the figure. The discrepancy indicates that the measurements of both cross sections with limited energy resolution and thermal rate coefficients at low temperatures are complementary and help clarify which model of IVR factors is more appropriate, that of Eqs. (4.4)–(4.7) or that of Eq. (4.8). There is also an apparent inconsistency between the present conclusions and the analysis of Rydberg electron transfer from Refs. 14 and 15 which was made with Eq. (4.8) and the parameters given. These experiments, such as the cross section measurements, had the problem of how to calibrate the measured relative rates. As our present measurements for rate coefficients of attachment of free electrons are more direct and consistent with the attachment cross sections of Refs. 18 and 19, they appear most trustworthy to us.

It appears also of interest to extend our modeling with the derived IVR factors P_l^{IVR} to attachment cross sections at higher electron energies and compare the results with measurements from this range such as summarized in Ref. 21. Figure 5 shows this comparison. The nearest agreement between modeling and experiments would be when smaller values of c_1 were chosen than for the low energy range. However, one can certainly not expect that the simple and empirical IVR factors of Eqs. (4.4)–(4.7) or Eq. (4.8) can be extended meaningfully to the large energy range of Fig. 5 and the corresponding large range of contributing l-values. We also abstain from an interpretation of the empirical IVR factors. Instead, we refer to Ref. 21 for attempts to relate differences between measured attachment cross sections up to energies of $E_{el}=10$ eV and classical finite-size attachment cross sections from Eq. (4.2) to the internal electronic structure of C_{60}^- (we note, however, that the analysis of Ref. 21 employed $\pi r_0^2=0.79$ nm^2 instead of $\pi r_0^2=0.394$ nm^2 such as used in the present work).

V. CONCLUSIONS

Rate coefficients for electron attachment to C_{60} have been measured in a FALP apparatus at 400 and 600 K using a relative rate method based on a comparison of negative and positive ion mass spectra for C_{60} and SF_6. The absolute values carry a large uncertainty (factor of 3) because of instrumental mass discrimination, but show that electron attachment to C_{60} occurs with a rate coefficient k_1 of $\sim 10^{-6}$ cm^3 s^{-1} with a small negative temperature dependence (Table I). The present experimental thermal attachment rate coefficients k_1, within our theoretical analysis, have been shown to be consistent with the experimental attachment cross section σ_{at} from Refs. 18 and 19. This analysis relied on modeling in terms of generalized Vogt–Wannier-type capture theory in the version elaborated in Refs. 27 and

28. The effects of the finite size of C_{60} (such as treated in Refs. 21 and 28) were analyzed and shown to be only of minor importance for small l. Furthermore, IVR factors in the form of Eqs. (4.4)–(4.7) were fitted to give an optimum internal consistency between the measured k_1 and σ_{at}. Our analysis of k_1 up to 1000 K illustrated the contributions from s-, p-, and d-waves. The present measurements are suggested to supersede those from Refs. 23 and 24 which apparently suffered from experimental problems and which were inconsistent with measured attachment cross sections. Our effective IVR factors differ from those derived in Refs. 4 and 22 on the basis of cross section data only. The combination of cross section and rate coefficient data, such as performed here, allowed us to go beyond the results of these earlier references. The importance of s-wave as well as higher partial wave contributions is documented, such as also done in several of the more recent discussions. An interpretation of these conclusions may be found in theoretical work such as Refs. 47–49.

ACKNOWLEDGMENTS

The AFRL authors are grateful for the support of the Air Force Office of Scientific Research for this work. J.F.F. was supported by the Air Force Research Laboratory Summer Faculty Program. N.S.S. was supported by the National Research Council Research Associateship Program. T.M.M. is under contract (Grant No. FA8718-04-C0006) to the Institute for Scientific Research of Boston College. J.T. is grateful for financial support of this work by EOARD (Grant Award No. FA8655-09-1-3001). Most helpful and critical discussions of the present manuscript by H. Hotop and E. E. Nikitin as well as technical help from A. I. Maergoiz are also gratefully acknowledged.

[1] J. Troe, T. M. Miller, and A. A. Viggiano, J. Chem. Phys. **127**, 244303 (2007).
[2] J. Troe, T. M. Miller, and A. A. Viggiano, J. Chem. Phys. **127**, 244304 (2007).
[3] H. Hotop, M.-W. Ruf, M. Allan, and I. I. Fabrikant, Adv. At., Mol., Opt. Phys. **49**, 85 (2003).
[4] I. I. Fabrikant and H. Hotop, Phys. Rev. A **63**, 022706 (2001).
[5] A. A. Viggiano, T. M. Miller, J. F. Friedman, and J. Troe, J. Chem. Phys. **127**, 244305 (2007).
[6] J. Rajput, L. Lammich, and L. H. Andersen, Phys. Rev. Lett. **100**, 153001 (2008).
[7] L. H. Andersen, Phys. Rev. A **78**, 032512 (2008).
[8] J. Troe, T. M. Miller, and A. A. Viggiano, J. Phys. Chem. **130**, 244303 (2009).
[9] J. U. Andersen, E. Bonderup, and K. Hansen, J. Phys. B **35**, R1 (2002).
[10] M. Lezius, P. Scheier, and T. Märk, Chem. Phys. Lett. **203**, 232 (1993).
[11] T. Jaffke, E. Illenberger, M. Lezius, S. Matejcik, D. Smith, and T. Märk, Chem. Phys. Lett. **226**, 213 (1994).
[12] S. Matejcik, T. D. Märk, P. Spanel, D. Smith, T. Jaffke, and E. Illenberger, J. Chem. Phys. **102**, 2516 (1995).
[13] A. Vostrikov, D. Y. Dubnov, and A. A. Agarkov, Tech. Phys. Lett. **21**, 517 (1995).
[14] J. Huang, H. S. Carman, and R. N. Compton, J. Phys. Chem. **99**, 1719 (1995).
[15] J. M. Weber, M.-W. Ruf, and H. Hotop, Z. Phys. D: At., Mol. Clusters **37**, 351 (1996).
[16] O. Elhamidi, J. Pommier, and R. Abouaf, J. Phys. B **30**, 4633 (1997).
[17] Y. V. Vasil'ev, R. R. Tuktarov, and V. A. Mazunov, Rapid Commun. Mass Spectrom. **11**, 757 (1997).
[18] A. A. Vostrikov, D. Yu. Dubnov, and A. A. Agarkov, High Temp. **39**, 22 (2001).
[19] V. Kasperovich, G. Tikhonov, and V. V. Kresin, Chem. Phys. Lett. **337**, 55 (2001).
[20] O. Elhamidi, J. Pommier, and R. Abouaf, Int. J. Mass Spectrom. **205**, 17 (2001).
[21] M. Lezius, Int. J. Mass Spectrom. **223–224**, 447 (2003).
[22] V. S. Prabhudesai, D. Nandi, and E. Krishnakumar, Eur. J. Phys. D **35**, 261 (2005).
[23] D. Smith, P. Spanel, and T. D. Märk, Chem. Phys. Lett. **213**, 202 (1993).
[24] D. Smith and P. Spanel, J. Phys. B **29**, 5199 (1996).
[25] J. U. Andersen, P. Hvelplund, S. B. Nielsen, U. V. Pedersen, and S. Tomita, Phys. Rev. A **65**, 053202 (2002).
[26] E. I. Dashevskaya, I. Litvin, E. E. Nikitin, and J. Troe, Phys. Chem. Chem. Phys. **10**, 1270 (2008).
[27] E. I. Dashevskaya, I. Litvin, E. E. Nikitin, and J. Troe, Phys. Chem. Chem. Phys. **11**, 9364 (2009).
[28] E. E. Nikitin and J. Troe, "Electron capture by finite-size polarizable molecules and clusters," Phys. Chem. Chem. Phys. (submitted).
[29] T. M. Miller, J. F. Friedman, A. E. S. Miller, and J. F. Paulson, Int. J. Mass Spectrom. Ion Process. **149/150**, 111 (1995).
[30] T. M. Miller, Adv. At., Mol., Opt. Phys. **51**, 299 (2005).
[31] J. F. Friedman, T. M. Miller, J. K. Friedman-Schaffer, A. A. Viggiano, G. K. Rekha, and A. E. Stevens, J. Chem. Phys. **128**, 104303 (2008).
[32] A. A. Viggiano, R. A. Perry, D. L. Albritton, E. E. Ferguson, and F. C. Fehsenfeld, J. Geophys. Res. **85**, 4551 (1980).
[33] R. Richter, P. Tosi, and W. Lindinger, J. Chem. Phys. **87**, 4615 (1987).
[34] Y. Ikezoe, S. Matsuoka, M. Takebe, and A. A. Viggiano, *Gas Phase Ion-Molecule Reaction Rate Constants Through 1986* (Maruzen, Tokyo, 1987).
[35] V. G. Anicich, "An Index of the Literature for Bimolecular Gas Phase Cation-Molecule Reaction Kinetics" (JPL Publication 3–19).
[36] G. Javahery, S. Petrie, J. Wang, and D. K. Bohme, Chem. Phys. Lett. **195**, 7 (1992).
[37] S. T. Arnold, S. Williams, I. Dotan, A. J. Midey, R. A. Morris, and A. A. Viggiano, J. Phys. Chem. **103**, 8421 (1999).
[38] A. J. Midey, S. Williams, S. T. Arnold, I. Dotan, R. A. Morris, and A. A. Viggiano, Int. J. Mass Spectrom. **195–196**, 327 (2000).
[39] A. A. Christodoulides and L. G. Christophorou, Chem. Phys. Lett. **61**, 553 (1979).
[40] E. Alge, N. G. Adams, and D. Smith, J. Phys. B **17**, 3827 (1984).
[41] R. Antoine, P. Dugourd, D. Rayane, E. Benichou, M. Broyer, F. Chandezon, and C. Guet, J. Chem. Phys. **110**, 9771 (1999).
[42] A. Ballard, K. Bonin, and J. Louderback, J. Chem. Phys. **113**, 5732 (2000).
[43] H. Yan, S. Yu, X. Wang, Y. He, W. Huang, and M. Yang, Chem. Phys. Lett. **456**, 223 (2008).
[44] P. A. Heiney, J. E. Fischer, A. R. McGhie, W. J. Romanow, A. M. Denenstein, J. P. McCauley, A. B. Smith, and D. E. Cox, Phys. Rev. Lett. **66**, 2911 (1991).
[45] J. M. Van Doren, T. M. Miller, A. A. Viggiano, P. Spanel, D. Smith, J. C. Bopp, and J. Troe, J. Chem. Phys. **128**, 094309 (2008).
[46] E. I. Dashevskaya, A. I. Maergoiz, J. Troe, I. Litvin, and E. E. Nikitin, J. Chem. Phys. **118**, 7313 (2003).
[47] F. A. Gianturco, R. R. Lucchese, and N. Sanna, J. Phys. B **32**, 2181 (1999).
[48] R. R. Lucchese, F. A. Gianturco, and N. Sanna, Chem. Phys. Lett. **305**, 413 (1999).
[49] F. A. Gianturco and R. R. Lucchese, J. Chem. Phys. **111**, 6769 (1999).